Environmental Pollution 391 (2026) 127581

Contents lists available at ScienceDirect

Environmental Pollution

journal homepage: www.elsevier.com/locate/envpol

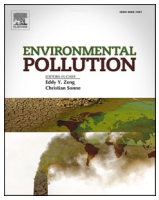

Size, spatial distribution, and diurnal variations of particulate nitrophenols in the central Yangtze River Delta, China: Implications for their emissions and atmospheric processes☆

Chao Qin [a], Jingyi Liu [b], Xinyu Ji [b], Wei Feng [b], Zhijuan Shao [c], Hong Liao [b], Yuhang Wang [d], Guofeng Shen [e], Mingjie Xie [b,*]

[a] Key Laboratory for Monitoring and Analysis of Organic Pollutants in Surface Water Environment of the Ministry of Ecology and Environment, Jiangsu Provincial Environmental Monitoring Center, Nanjing, 210019, China
[b] Collaborative Innovation Center of Atmospheric Environment and Equipment Technology, Jiangsu Key Laboratory of Atmospheric Environment Monitoring and Pollution Control, School of Environmental Science and Engineering, Nanjing University of Information Science & Technology, Nanjing, 210044, China
[c] School of Environment Science and Engineering, Suzhou University of Science and Technology, Shihu Campus, Suzhou, 215009, China
[d] School of Earth and Atmospheric Sciences, Georgia Institute of Technology, Atlanta, GA, 30332, United States
[e] Laboratory for Earth Surface Processes, College of Urban and Environmental Sciences, Peking University, Beijing, 100871, China

ARTICLE INFO

Keywords:
Nitrophenols
Fine PM
Spatial variability
Diurnal pattern
Source apportionment

ABSTRACT

In this study, paired integrated $PM_{2.5}$ and PM_{10} samples, as well as time-resolved $PM_{2.5}$ samples, were collected during summer and winter from two sampling campaigns in northern Nanjing, China. Synchronous wintertime $PM_{2.5}$ samples from five urban sites in the center of the Yangtze River Delta (YRD), China, were retrieved from another campaign. Four nitrophenols (NPs)—4-nitrophenol (4NP), 3-methyl-4-nitrophenol (3M4NP), 2-methyl-4-nitrophenol (2M4NP), and 4-nitrocatechol (4NC)—were speciated in each sample. The concentrations of individual NPs in $PM_{2.5}$ and PM_{10} were significantly correlated ($r > 0.70$, $p < 0.05$), and the majority (>70 %) of the four NPs were present in fine particles. All NPs showed similar temporal variations across the five urban sites in winter ($r = 0.68 \pm 0.15$–0.78 ± 0.066, $p < 0.05$), with 4NC exhibiting the least spatial variability. The diurnal variations of $PM_{2.5}$-bound 4NP, 3M4NP, and 2M4NP in winter showed two elevations during 8:00–14:00 and 16:00–2:00 (next day), likely dominated by the photooxidation of gaseous aromatics and nighttime NO_3· chemistry, respectively. In summer, their diurnal patterns were characterized by a sharp increase during 16:00–20:00 and rapid removal after 20:00, which may correspond to NP formation from newly emitted precursors during rush hour and NO_3·-initiated degradation at night. The diurnal variations of 4NC were similar to those of anhydrosugars in winter and secondary sulfate in summer. By combining measurement data of NPs and source tracers in $PM_{2.5}$, positive matrix factorization (PMF) was conducted to evaluate NP sources. A secondary NP production factor was identified as the largest contributor to total NPs in time-resolved samples for both summer (71.4 %) and winter (39.3 %). The biomass burning factor contributed significant fractions of NPs in all winter samples, particularly for 4NC (>80 %).

1. Introduction

Nitrophenols (NPs) are ubiquitous in the atmosphere and are characterized by a benzene ring substituted with at least one nitro group and one hydroxyl group. Evidence shows that exposure to NPs can affect plant growth (Abdelmoneim et al., 2024; Adamek et al., 2024) and is associated with several negative health outcomes in humans (e.g., inflammation and respiratory distress; Eichenbaum et al., 2009; Khan et al., 2022; Mo et al., 2024). In addition, NPs are strong chromophores that absorb sunlight in the near UV and shorter visible wavelengths (Laskin et al., 2018), which is a characteristic optical property of "brown carbon" (BrC). Field measurements and laboratory experiments have found that the contribution of NPs to the light absorption of organic carbon (OC) is several times higher than their mass contribution (Mohr

☆ This paper has been recommended for acceptance by Prof. Pavlos Kassomenos

* Corresponding author. 219 Ningliu Road, Nanjing, Jiangsu, 210044, China.
E-mail addresses: mingjie.xie@nuist.edu.cn, mingjie.xie@colorado.edu (M. Xie).

https://doi.org/10.1016/j.envpol.2025.127581
Received 1 October 2025; Received in revised form 1 December 2025; Accepted 22 December 2025
Available online 23 December 2025

et al., 2013; Li et al., 2020b; Xie et al., 2017, 2019a; 2020).

To better evaluate the phytotoxicity, health risks, and radiative effects of NPs, their origins, environmental transport, and transformations have been widely investigated. Combustion experiments have shown that the primary emission sources of ambient NPs contain biomass burning (Lin et al., 2016; Wang et al., 2017), coal combustion (Lu et al., 2019a), and motor vehicle exhaust (Inomata et al., 2015; Lu et al., 2019b). In addition, NPs in the particle phase can form through daytime photooxidation of volatile aromatic organics (e.g., phenols, benzene, and toluene) in the presence of NO_X (Nakayama et al., 2010; Lin et al., 2015; Liu et al., 2016) and nighttime NO_3·-initiated oxidation (Wang and Li, 2021; Zhang et al., 2025), followed by partitioning of gaseous products to particulate organic matter or aerosol liquid water (ALW). The nitration of dissolved aromatics in ALW is another important formation pathway for secondary NPs (Barzaghi and Herrmann, 2004; Vidović et al., 2018; Pang et al., 2019). Based on the speciation of NPs in laboratory simulations of combustion and secondary organic aerosol (SOA) formation, several source-specific NPs have been identified. For example, NPs in biomass burning emissions are featured by a structure of methoxy nitrophenol (Xie et al., 2019a); nitrophloroglucinol is derived from the oxidation of only benzene in chamber experiments with various volatile aromatic compounds (Xie et al., 2017). However, these compounds are rarely observed in field measurements, possibly due to their short atmospheric lifetimes. Although motor vehicle emissions and coal combustion are enriched with 4-nitrophenol and nitrocatechols/methyl nitrocatechols, respectively (Lu et al., 2019a, b), these compounds are also generated from biomass burning and SOA formation (Xie et al., 2017, 2019a). Therefore, the commonly identified NPs in the atmosphere, including nitrophenols, methyl nitrophenols, nitrocatechols, and methyl nitrocatechols, can hardly be used to apportion NPs to specific sources.

According to previous field studies, particulate NPs exist primarily in the fine mode in Qingdao, China, during winter (Liang et al., 2020; Guo et al., 2024) and in Mainz, Germany (Zhang et al., 2010). Li et al. (2016) observed significant fractions of NPs, except for 4-nitrocatechol, in coarse particles during severe haze episodes in Shanghai. The mean concentrations of NPs in winter were several times to orders of magnitude higher than in summer (Kahnt et al., 2013; Chow et al., 2015; Yuan et al., 2021), which can be attributed to increased primary emissions of NPs and their precursors, weaker degradation, lower planetary boundary layer height (PBLH), and the partitioning of gaseous NPs to the particle phase at lower temperatures in winter. Multiple-site observations showed that urban areas with stronger anthropogenic emissions had higher mean NP concentrations than rural or remote areas (Wang et al., 2018). Because oxidants and reactants in air pass through filters continuously during air sampling, particulate NPs may undergo chemical transformations on filters during long-term (12–24 h) sampling. Short-term (1–2 h) sampling or real-time mass spectrometry analysis are alternative methods for investigating NPs in the atmosphere. Time-resolved measurements showed that the diurnal pattern of NPs was characterized by a prominent nighttime peak in fall and winter (Sakakibara et al., 2022; Guo et al., 2024) and during the crop residue burning season (Wang et al., 2020), which was attributed to NO_3·-initiated oxidation of aromatic precursors.

Due to the complex sources and transformation pathways, the ambient concentrations of NPs were not well revealed. For example, the size distribution and spatiotemporal variations of NPs have rarely been investigated within the same region, which could provide important insights into their main sources. Moreover, there is a relative dearth of studies evaluating the contributions of NP sources using highly specific tracers for organic aerosols. In this study, filter samples of atmospheric particles were collected from three sampling campaigns in our previous work. These samples were analyzed for NPs to illustrate their size, spatial distribution, and diurnal variations in the central area of the Yangtze River Delta, China. Other compositional data, including water-soluble inorganic ions (WSIIs) and organic molecular markers (OMMs), from the same samples were obtained for comparison and source apportionment using the positive matrix factorization (PMF) model. The study results will shed light on the relative importance of primary emissions and secondary formation for particulate NPs and support the evaluation of their health and climate effects.

2. Methods

2.1. Sample collection

In this study, filter samples of ambient particulate matter (PM) were collected from three completed sampling campaigns. Detailed information on the sampling methods is provided in Feng et al. (2023, 2024) and Cui et al. (2025). Briefly, $PM_{2.5}$ and PM_{10} sample pairs were collected at Nanjing University of Information Science and Technology (NUIST, 32.21° N, 118.71° E; Fig. S1 in Supplementary Information) in northern Nanjing, China, where two identical samplers (Laoying 2030, Longying Environmental, China) equipped with 2.5 μm and 10 μm cut-point impactors, respectively, were operated at a flow rate of 100 L min^{-1}. Eleven-hour samples were collected during 8:00–19:00 (daytime) and 20:00–7:00 (overnight, nighttime) in summer 2020 and winter 2020/2021.

During winter 2020/2021 (11/27/2020–02/28/2021), $PM_{2.5}$ samples were also collected in five central cities of the YRD region in China: Nanjing, Suzhou, Wuxi, Changzhou, and Zhenjiang (Fig. S1). A four-channel sampler (TH-16a, Wuhan Tianhong, China) was operated at a flow rate of 16.7 L min^{-1} from 10:00 to 9:00 the next day for each sampling day. Sampling was conducted at urban sites at the same time every three days in the five cities.

Time-resolved $PM_{2.5}$ samples were collected at the NUIST site in January (winter) and July–August (summer) 2019. Two identical samplers ($PM_{2.5}$-PUF-300, Mingye Environmental, China) equipped with 2.5 μm cut-point impactors were operated alternately at a flow rate of 300 L min^{-1}. Sampling was conducted at 2-h intervals from 8:00 to 20:00 and 6-h intervals from 20:00 to 8:00 the next day, resulting in eight filter samples per sampling day. Ambient temperature (°C) and relative humidity (RH, %) data recorded during each sampling interval were obtained from Feng et al. (2023), and hourly gaseous pollutant data (e.g., NO_2) were retrieved using the same method as Yu et al. (2019) from a nearby monitoring station.

As shown in Fig. S1, all sampling sites are located in the center of the YRD, one of the most developed regions in China. Feng et al. (2024) found that the contributions of major OC sources (regional biomass burning and fossil fuel combustion) in this area were homogeneously distributed. All PM samples were collected on quartz fiber filters pre-baked at 550 °C for 4 h to eliminate potential contamination. The PM samples from the three campaigns were analyzed to determine the size distribution, spatial variability, and diurnal variations of NPs in central

Table 1
Information on PM samples analyzed for size, spatial distribution, and diurnal variations of NPs in this study.

	Size distribution	Spatial distribution	Diurnal variation
Sampling site	NUIST	Five urban sites in Nanjing, Suzhou, Wuxi, Changzhou, and Zhenjiang	NUIST
Sampling period	Summer: 2020/07/24–2020/08/20; Winter: 2020/12/19–2021/01/17	Winter: 2020/11/27–2021/02/28;	Summer: 2019/07/24–2019/08/21; Winter: 2019/01/12–2019/01/20
PM size	$PM_{2.5}$ and PM_{10}	$PM_{2.5}$	$PM_{2.5}$
Sample No.	Summer: 48 pairs; Winter: 48 pairs	32 at each site	Summer: 56 (7 days); Winter: 56 (7 days)

YRD. More information on the sampling dates and sample numbers is provided in Table 1.

2.2. Chemical analysis of NPs

The methods for filter pretreatment and instrumental analysis of NPs were similar to those used for polar OMMs in previous studies (Feng et al., 2023, 2024; Cui et al., 2025). Briefly, an aliquot of each filter sample was cut into pieces and spiked with 40 μL of isotopically labeled 4-nitrophenol (10 ng μL^{-1} of 4-nitrophenol-D4 in methanol) as the internal standard (IS). The sample pieces were ultrasonically extracted in a mixture of methanol and dichloromethane (DCM; 1:1, v/v) for 15 min twice. After that, the filter extracts were filtered, rotary evaporated, and dried under a stream of nitrogen gas. Then, NPs in the dried extracts were reacted with 50 μL of N, O-bis(trimethylsilyl)trifluoroacetamide (BSTFA): trimethylchlorosilane (TMCS; 99:1) and 10 μL pyridine at 70 °C for 3 h to convert –OH and –COOH groups into the corresponding trimethylsilyl esters and ethers. Prior to instrumental analysis, 340 μL of pure hexane was added to dilute the NP derivatives to a final volume of 400 μL.

An aliquot of 2 μL of each sample extract solution was injected for analysis using gas chromatography (GC; Agilent 7890, United States) – mass spectrometry (MS; Agilent 5977, United States) under splitless mode. GC separation was performed with an Agilent HP-5 ms capillary column (30 m × 0.25 mm × 0.25 μm), and the temperature was programmed from 50 °C (held for 2 min) to 120 °C at 3 °C min^{-1} (held for 0 min), then to 300 °C at 6 °C min^{-1} (held for 10 min). Six-point calibration curves were generated to quantify NPs in extract solutions using the IS method. In Table S1 of the Supplementary Information, twelve authentic standards of NPs were obtained from AccuStandard (United States) and Sigma-Aldrich (United States), but only four—4-nitrophenol (4NP), 3-methyl-4-nitrophenol (3M4NP), 2-methyl-4-nitrophenol (2M4NP), and 4-nitrocatechol (4NC)—were identified in most PM samples and are reported here. Recoveries were determined by analyzing blank filters spiked with known amounts of target NPs, and the method detection limit (MDL) was calculated as three times the standard deviation of multiple injections ($n = 6$) at the lowest calibration level. As shown in Table S1, the mean recoveries of 4NP, 3M4NP, 2M4NP, and 4NC ranged from 70.1 % to 111 % and were not used to adjust their concentrations in PM samples. The extremely low recoveries of some NPs (e.g., 2-nitrophenol and 2-nitrophloroglucinol) might be ascribed to the low derivatization efficiency of the ortho-phenolic hydroxy group. Field blank samples were analyzed identically to account for potential contamination.

To evaluate the sources, formation, and light absorption of NPs, concentrations of other components in PM samples, including WSIIs (NH_4^+, Ca^{2+}, NO_3^-, and SO_4^{2-}), OC, elemental carbon (EC), non-polar and polar OMMs, and the light absorption coefficient of methanol-extractable OC (MEOC) at 365 nm (Abs_{365}), were obtained from Feng et al. (2023, 2024, 2025) and Cui et al. (2025) for comparison. The contributions of the target NPs to Abs_{365} were estimated as the product of their ambient concentrations and the corresponding mass absorption efficiency at 365 nm (MAE_{365}, m^2 g^{-1}; Table S1). The MAE_{365} values were determined by measuring the light absorbance of methanol solutions of individual NPs in the same manner as Xie et al. (2017). In Table S2, the non-polar and polar OMMs are grouped by vapor pressures at 298.15 K ($p^{o,*}_L$) and by origins, respectively, as in the studies mentioned above. Table S3 provides the mean concentrations of bulk PM components (WSIIs, OC, and EC) and OMM groups in integrated PM samples from northern Nanjing and the five urban sites in central YRD. Fig. S2–S4 illustrate their diurnal variations in northern Nanjing in summer and winter 2019.

2.3. PMF modeling

The identification and quantification of NP sources were achieved by combining concentration data of NPs and other PM components listed in Table S2 as input for the EPA PMF 5.0 model. Due to the limited sample size, the compositional data of $PM_{2.5}$ samples from the three sampling campaigns were combined, and grouped OMMs were used instead of individual species. Because source profiles of PM can change significantly by season, PMF analysis was conducted separately for summer and winter data. Except for EC, whose temporal variations in summer might be uncertain due to its low concentrations (<1 μg m^{-3}) in many summer samples, all other bulk components and grouped OMMs were included in the PMF analysis. After excluding samples with no OMM data, the resulting PMF data sets for summer (PMFs) and winter (PMFw) consisted of 104 and 252 observations, respectively, of 23 species (4NP, 3M4NP, 2M4NP, 4NC, 5 bulk components, and 14 OMM groups; Tables S2 and S4). The final number of factors was determined by considering the physical meaningfulness of the output factors, the robustness of PMF solutions with factors ranging from 4 to 12, and the changes in Q/Q_{exp} with the factor number (Tables S5 and S6). More details on data preparation and factor number determination for PMF analysis are provided in Text S1 in the Supplementary Information.

3. Results and discussion

3.1. NPs in $PM_{2.5}$ and PM_{10} from northern Nanjing

Among the four identified NPs, 4NP was the most abundant compound, followed by 4NC, 2M4NP, and 3M4NP (Fig. S5 and Table 2), consistent with observations in Xi'an, China (Yuan et al., 2021). However, 4NC showed higher mean concentrations than 4NP in Hong Kong, China (Chow et al., 2015), and in many other cities in western countries (Table 2; Zhang et al., 2010; Kahnt et al., 2013; Mohr et al., 2013; Zhang et al., 2013; Xie et al., 2019b). Except for 4NC in Mainz, Germany, a seasonal cycle of lower concentrations in summer and higher concentrations in winter was observed for NPs in all the cities listed in Table 2. In addition to changes in meteorological conditions (e.g., temperature, solar radiation, and PBLH), emissions of NPs and their precursors were more intensive in winter than in summer. For example, more biomass and fossil fuels are burned in winter for domestic heating (Qi and Wang, 2019).

As shown in Table 2 and Fig. S5, more than 70 % of the four NPs in PM_{10} were accounted for by $PM_{2.5}$, and their concentrations in $PM_{2.5}$ and PM_{10} are significantly correlated in both summer ($r = 0.75$–0.93, $p < 0.01$) and winter ($r = 0.94$–0.96, $p < 0.01$), indicating that particulate NPs are mainly distributed in fine particles in northern Nanjing. Because the Abs_{365} of MEOC is also enriched in fine particles, the mean contributions of total NPs in $PM_{2.5}$ and PM_{10} to Abs_{365} of MEOC were very close in both summer ($PM_{2.5}$ 0.58 % ± 0.45 %, PM_{10} 0.67 % ± 0.43 %) and winter (~2 %). Although low molecular weight (MW) NPs are strong light-absorbing chromophores, they are not the main components of BrC in northern Nanjing. Due to the evaporation of NPs at higher temperatures, significantly greater ($p < 0.01$) coarse fractions of NPs were observed in summer (23.6 % ± 18.3 %) than in winter (10.3 % ± 7.91 %). The mean concentrations of 4NP in $PM_{2.5}$ (summer, 1.67 ± 1.05 ng m^{-3}; winter 25.7 ± 12.9 ng m^{-3}) and PM_{10} (2.08 ± 1.32 ng m^{-3}; 29.8 ± 13.6 ng m^{-3}) differed significantly (Student's t-test, $p < 0.01$) in both summer and winter. Sakakibara et al. (2022) reported a mean particle phase fraction (F_p) of 33 % ± 11 % for 4NP in Kumamoto, Japan, indicating the presence of substantial 4NP in the gas phase. The associations of NPs with coarse PM were probably caused by the adsorption and condensation of vapor-phase NPs (Offenberg and Baker, 1999; Wang et al., 2009) and heterogeneous formation on coarse PM (Liang et al., 2020). However, the fractions of 4NP in $PM_{2.5}$ in this study (>80 %) during summer were higher than those in urban Jinan (<60 %), China (Li et al., 2020a). One possible explanation is that the relative humidity (RH, %) during the same period as the NP measurement in northern Nanjing in summer (81.6 % ± 16.0 %; Wang, 2013) was higher than in Jinan (57.7 % ± 12.2 %; Li et al., 2020a), and the dissolution of

Table 2
Mean concentrations of target NPs in central YRD cities (this study) and other studies.

City, country	Site type	Period	PM Size	4NP	3M4NP	2M4NP	4NC	References
Nanjing, China	Suburban	Summer 2020	<2.5 μm	1.67 ± 1.05	0.20 ± 0.13	0.63 ± 0.50	0.88 ± 0.56	this study
			<10 μm	2.08 ± 1.32	0.28 ± 0.21	0.86 ± 0.99	1.01 ± 0.85	
		Winter 2020–2021	<2.5 μm	25.7 ± 12.9	4.43 ± 2.09	7.16 ± 2.80	7.78 ± 5.15	
			<10 μm	29.8 ± 13.6	4.68 ± 2.60	7.94 ± 3.63	6.42 ± 4.20	
Nanjing, China	Urban	Winter 2020–2021	<2.5 μm	9.84 ± 4.92	1.14 ± 0.63	2.34 ± 2.12	5.02 ± 6.49	
Suzhou, China			<2.5 μm	14.8 ± 7.80	1.14 ± 0.57	2.20 ± 1.24	5.25 ± 5.34	
Wuxi, China			<2.5 μm	13.2 ± 6.97	1.57 ± 0.85	3.11 ± 2.51	5.69 ± 6.15	
Changhzou, China			<2.5 μm	20.4 ± 13.1	2.76 ± 1.83	4.76 ± 3.51	9.04 ± 9.89	
Zhenjiang, China			<2.5 μm	8.59 ± 4.21	1.33 ± 0.70	2.16 ± 1.20	5.20 ± 4.72	
Xi'an, China	Urban	Summer 2016	<2.5 μm	0.45 ± 0.28	0.070 ± 0.060	0.10 ± 0.10	0.16 ± 0.11	Yuan et al. (2021)
		Winter 2015	<2.5 μm	15.6 ± 6.60	3.40 ± 1.52	4.50 ± 1.72	15.5 ± 7.40	
Hong Kong, China	Urban	Summer 2010–2012	<2.5 μm	0.31 ± 0.22	0.020 ± 0.0072	0.18 ± 0.13	0.77 ± 0.71	Chow et al. (2015)
		Winter 2009–2012	<2.5 μm	1.71 ± 0.99	0.14 ± 0.090	1.06 ± 0.067	3.98 ± 2.95	
Xianghe, China	Rural	Summer 2013	<10 μm	0.98 ± 0.78	0.09 ± 0.07	0.32 ± 0.21	/	
Wangdu, China	Rural	Summer 2014	<10 μm	2.63 ± 2.66	0.21 ± 0.35	0.68 ± 0.78	/	
Melpitz, Germany	Rural	Summer 2014	<10 μm	0.06 ± 0.03	0.03 ± 0.00	0.04 ± 0.00	/	Teich et al. (2017)
TROPOS, Germany	Urban	Winter 2014	<10 μm	7.09 ± 7.08	2.60 ± 2.22	3.64 ± 3.05	/	
Melpitz, Germany	Rural	Winter 2014	<10 μm	4.09 ± 3.27	2.44 ± 2.20	3.64 ± 3.06	/	
Mainz, Germany	Suburban	Summer 2006	<3 μm	1.69 ± 1.27	/	/	6.88 ± 7.53	Zhang et al. (2010)
			TSP	2.57 ± 2.32	/	/	8.22 ± 7.98	
		Winter 2006–2007	<3 μm	3.96 ± 2.88	/	/	4.18 ± 2.99	
			TSP	5.28 ± 3.54	/	/	4.50 ± 3.20	
Pasadena, United States	Urban	Summer 2010	<2.5 μm	/	1.24[a]		1.67	Zhang et al. (2013)
Research triangle park, United States	Suburban	Summer 2013	<2.5 μm	0.018 ± 0.027	0.0068 ± 0.0092[a]		0.057 ± 0.042	Xie et al. (2019b)
Hamme, Belgium[b]	Rural	Summer 2010	<10 μm	0.29[c]	/	/	0.23	Kahnt et al. (2013)
		Winter 2010–2011	<10 μm	1.19[c]	/	/	11.6	
Detling, United Kingdom	Rural	Winter 2012	<3 μm	0.02[c]	5[a]		2.5	Mohr et al. (2013)

[a] Including all isomers with MW of 152.035.
[b] Median values.
[c] Including all isomers with MW of 138.019.

4NP in aerosol liquid water would enhance its fraction in fine PM.

The correlations of individual NPs with other PM components, including bulk species and OMM groups, in northern Nanjing are shown using contour plots in Fig. S6. In summer, NP concentrations in $PM_{2.5}$ and PM_{10} were moderately correlated with both bulk PM components and anhydrosugars (Fig. S6a and c). In winter, less volatile *n*-alkanes (lg $p_L^{o,*} > -8$) and oxy-PAHs showed stronger correlations with NPs than anhydrosugars (Fig. S6b and d), indicating that NPs in northern Nanjing had multiple origins and cannot be used as tracers for specific emission sources or formation pathways. This may explain why many studies

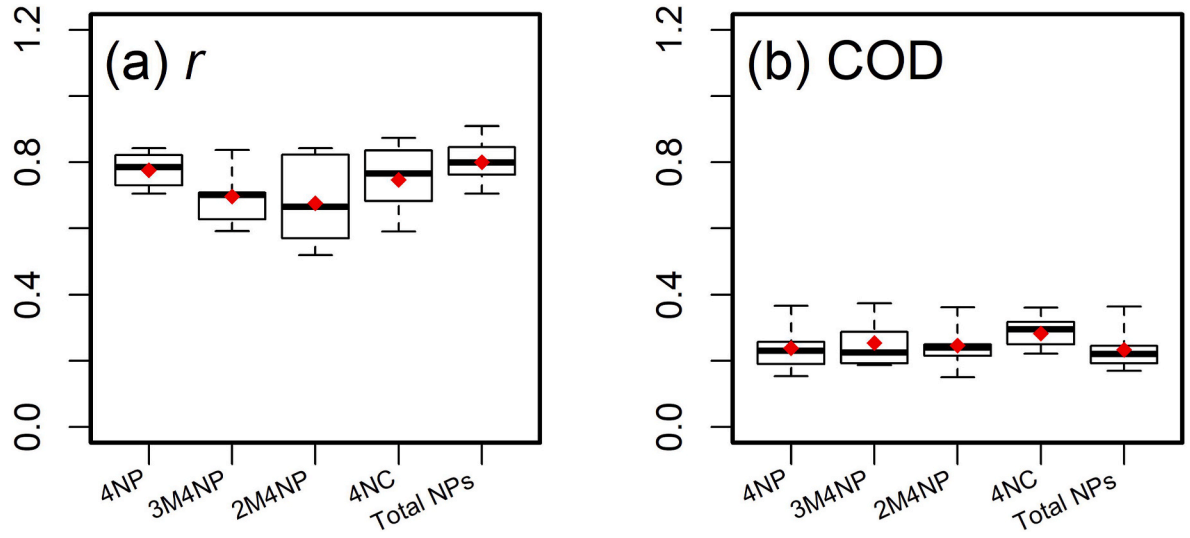

Fig. 1. Distribution of (a) correlation coefficients (*r*) and (b) coefficients of divergence (COD) for concentrations of individual NPs between two sampling sites in the five central cities of the YRD region
The boxes depict the median (dark line), interquartile range (box), 10th and 90th percentiles (whiskers), and mean (red diamond) of *r* and COD for 10 pairs of sampling sites. (For interpretation of the references to colour in this figure legend, the reader is referred to the Web version of this article.)

identified sources of NPs using compounds with known origins (e.g., SO_2, O_3, and levoglucosan; Kahnt et al., 2013; Li et al., 2016; Wang et al., 2018; Li et al., 2020a). However, OMM-based source apportionment of NPs has rarely been conducted.

3.2. Spatial distribution of $PM_{2.5}$-bound NPs in central YRD

Mean concentrations of the four NPs in $PM_{2.5}$ from the five cities in central YRD followed the same order (4NP > 4NC > 2M4NP > 3M4NP) as those from northern Nanjing (Table 2). Changzhou had the highest total concentrations of NPs (36.1 ± 27.1 ng m^{-3}) among the five cities in winter, followed by Wuxi (23.6 ± 15.5 ng m^{-3}) and Suzhou (22.9 ± 14.1 ng m^{-3}). To evaluate the spatial variability of NP concentrations in the central YRD region, the correlation coefficients (r) and coefficients of divergence (COD, 0–1; Kim et al., 2005; Wilson et al., 2005; Wongphatarakul et al., 1998) for concentrations of individual NPs between sampling sites are shown in Fig. 1. In general, the concentrations of all NPs showed significant correlations ($r = 0.68 \pm 0.15$–0.78 ± 0.066, $p < 0.05$) between sampling sites across the five cities, and their mean COD values (0.24 ± 0.097–0.28 ± 0.069) were close to the empirical threshold (0.20; Krudysz et al., 2008) for homogeneous spatial distribution. Thus, the four target NPs in the five central cities of YRD likely had similar temporal variations in winter and were influenced by regional sources. However, the significantly ($p < 0.05$) higher concentrations of individual NPs in Changzhou suggested stronger local emissions or formation. Feng et al. (2024) found that the contribution of traffic-related factors, which had the highest spatial variability, to OC in Changzhou (37.3 %) was higher than in the other four cities (16.1 %–25.6 %) due to stronger local emissions. Differences in local mixing and boundary layer dynamics across the five cities may also contribute to the spatial variability of NPs. Similar to the observations in northern Nanjing, the target NPs accounted for only 1.20 % ± 0.53 %–1.97 % ± 0.96 % Abs_{365} of MEOC in $PM_{2.5}$ samples from the five urban sites in central YRD.

Concentrations of all NPs were strongly intercorrelated at each of the five urban sites in central YRD during winter (Fig. S7). The strong correlations between NPs and various OMMs (e.g., *n*-alkanes, oxy-PAHs, and anhydrosugars) support that individual NPs are not specifically related to particular sources. Fig. S8 compares the mean concentrations of $PM_{2.5}$-bound NPs from northern and downtown Nanjing during the eight overlapping sampling days in winter 2020–2021. Concentrations of 3MNP, 2M3NP, and 4NC at the two sites were significantly correlated ($r = 0.85$–0.99, $p < 0.05$), and only 4NC showed no significant ($p = 0.83$) difference in mean concentrations. In addition, excluding Changzhou, the mean concentrations of 4NC had the smallest difference across the other four urban sites in central YRD (5.02 ± 6.49–5.69 ± 6.15 ng m^{-3}; Table 2). These results may indicate that 4NC has the lowest spatial variability in central YRD. Wang et al. (2018) measured $PM_{2.5}$-bound NPs at four sites in northern China and observed large spatial variability in total NPs (2.5 ± 1.6–9.8 ± 4.2 ng m^{-3}). This is because the four sites were of different types (urban, rural, and mountain) and distributed over a broader region (Hebei and Shandong provinces).

3.3. Diurnal variations of NPs in $PM_{2.5}$ from northern Nanjing

In Fig. 2, the diurnal patterns of 4NP, 3M4NP, and 2M4NP showed two elevations during 8:00–14:00 and 16:00–2:00 (next day) in winter. After sunrise, increased temperature (Fig. S9a), along with higher PBLH and stronger solar radiation, led to lower concentrations of particulate NPs through dilution, photolysis, and evaporation. As such, the first elevation before 14:00 was supposed to be caused by the rapid formation of NPs due to increased atmospheric oxidation capacity (Fig. S9d).

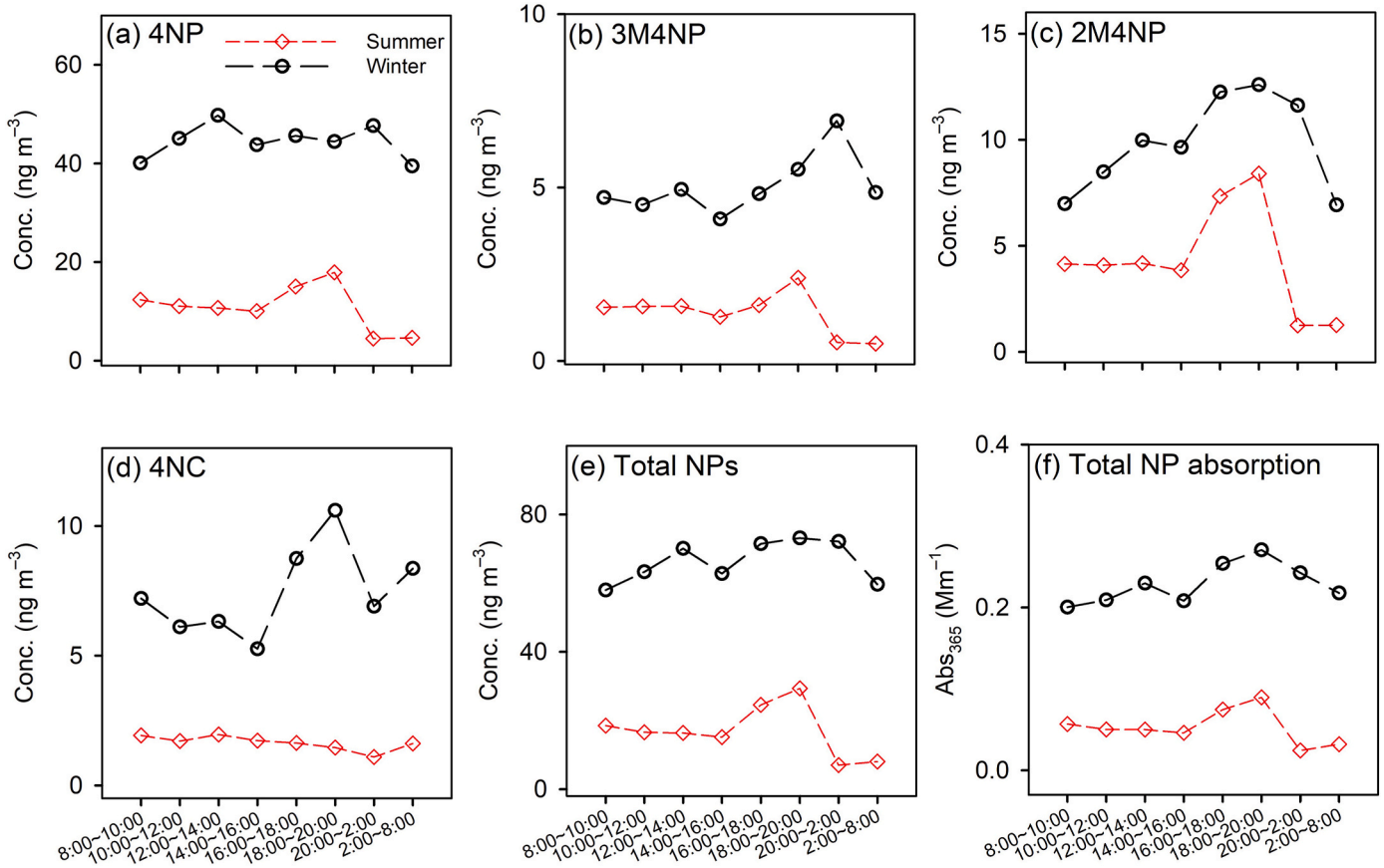

Fig. 2. Diurnal variations in mean concentrations of individual NPs and their contributions to Abs_{365} in $PM_{2.5}$ from northern Nanjing in summer and winter 2019.

Chamber experiments have demonstrated that NPs can form through the photooxidation of volatile aromatic compounds in the presence of NO_X (Nakayama et al., 2010; Lin et al., 2015; Liu et al., 2016; Xie et al., 2017). In the afternoon, the second increase in particulate NPs was possibly initiated by the decline in PBLH and temperature and was promoted by primary emissions from motor vehicles during rush hour (Fig. S9c) and biomass burning for domestic heating (Fig. S4c). Additionally, the peak concentrations at 20:00–2:00 can be explained by NO_3·-induced oxidation of aromatic precursors (Wang and Li, 2021; Zhang et al., 2025), and the increase in RH at night (Fig. S9b) facilitated the dissolution of gaseous NPs in ALW. Nighttime peak concentrations of NPs were also observed in northern and eastern China (Wang et al., 2020; Guo et al., 2024) and Kumamoto, Japan (Sakakibara et al., 2022). Among other PM components, only NO_3^- exhibited a similar increase from afternoon to midnight with the same peak time (Fig. S2c), and the rise in mean NO_2 concentration that began during afternoon rush hours continued until 2:00 (Fig. S9c), supporting the role of NO_3· chemistry in NP formation at night.

The diurnal variation of 4NC in winter was similar to that of anhydrosugars (Fig. 2d and S4c). Its mean concentration decreased from 8:00 to 16:00 and showed a prominent increase from 16:00 to 20:00. Although 4NC can also form through the photooxidation of aromatic compounds, the ·OH oxidation rate of 4NC is an order of magnitude higher than that of 4NP (Zhao et al., 2015), which may reveal the decrease of 4NC during the daytime. The significant increase of 4NC during the same period (16:00–20:00) as PAHs and anhydrosugars was likely attributed to the impact of combustion emissions (e.g., biomass burning) for domestic heating in winter. Unlike the other three NPs, NO_3·-induced oxidation is a degradation pathway rather than a formation mechanism during 20:00–2:00 in winter. Because 4NP dominated the mean concentrations among the four NPs, the diurnal pattern of total NPs was driven by 4NP (Fig. 2e). However, the contribution of total NPs to Abs_{365} (0.20 ± 0.10–0.27 ± 0.10 Mm^{-1}) peaked at 18:00–20:00 in winter (Fig. 2f), reflecting the influence of 4NC due to its high MAE_{365} value (8.48 $m^2\ g^{-1}$; Table S1).

In summer, 4NP, 3M4NP, and 2M4NP exhibited almost identical diurnal patterns (Fig. 2a–c). Their mean concentrations remained relatively constant from 8:00 to 16:00, then rose substantially until 20:00, followed by a sharp decrease overnight. The nearly flat daytime pattern of these three species may result from a balance between secondary formation and removal processes in summer. The spike from 16:00 to 20:00 was expected to be caused by the formation of NPs from newly emitted precursors during rush hours (Fig. S9c) and the partitioning of gaseous NPs to the particle phase at lower temperatures (Fig. S9a). Unlike in winter, mean NO_2 concentration decreased earlier after 20:00 in summer (Fig. S9c). Due to the lack of primary emissions, NO_3·-induced oxidation became a degradation pathway at night, leading to the rapid removal of 4NP, 3M4NP, and 2M4NP. The diurnal variation of mean concentrations of 4NC in summer was very different (Fig. 2d), but resembled those of NH_4^+ and SO_4^{2-} (Fig. S2a and d). Therefore, it was assumed that 4NC was formed through aqueous-phase oxidation in summer. Since the mean concentrations of 4NC were much lower than those of 4NP and varied less significantly, the diurnal variations of both total NPs and their Abs_{365} contributions were similar to those of 4NP, 3M4NP, and 2M4NP in summer. Including the diurnal cycles, except for 4NC in winter, little or no correlation was observed between NPs and anhydrosugars (Fig. S10). Less intercorrelation between 4NC and the other three NPs was observed for time-resolved samples than for integrated PM samples. These results suggest that ambient NPs may not be directly emitted from biomass burning or share the same formation pathways.

3.4. Source apportionment

Based on the interpretability and robustness of the resulting factors from the 4- to 12-factor solutions, the 8- and 9-factor solutions were selected for the PMFs and PMFw data, respectively (Text S1; Tables S5 and S6). Since the compositional data of $PM_{2.5}$ samples have been used for source apportionment of organic aerosols, the associations of the factors shown in Fig. 3 with emission sources or atmospheric processes were identified through the characteristic species in each factor profile and by comparison with previous studies (Xie et al., 2022; Feng et al., 2023, 2024; Cui et al., 2025).

Both the PMFs and PMFw solutions include six factors linked to biomass burning (characteristic species: anhydrosugars), coal burning (PAHs), dust (Ca^{2+}), lubricating oil combustion (steranes and hopanes), nitrate (NO_3^-), and secondary NP production (4NP, 3M4NP, and 2M4NP; Fig. 3). Although the PMFs solution separated isoprene and α-pinene SOA tracers into two factors, the isoprene SOA tracers were lumped with NH_4^+ and SO_4^{2-} (Fig. 3g). Since isoprene SOA tracers and sulfate are both secondary products, and inorganic sulfate participates in the formation of isoprene SOA (e.g., 2-methyltetrols; Surratt et al., 2010; Cui et al., 2018), these two groups of species had some similarity in diurnal variations during daytime in summer (Figs. S2a and S4a). Besides α-pinene SOA tracers, the α-pinene SOA factor in the PMFs solution also contained nearly 50 % of sugar alcohols and saccharides (Fig. 3h). This is because sugar polyols are mainly associated with microbiota activity during the growing season (Simoneit et al., 2004; Verma et al., 2018) and exhibited similar diurnal patterns as α-pinene SOA tracers (Fig. S4). The biogenic SOA factor from the PMFw solution was characterized by high loadings of both isoprene and α-pinene SOA tracers and also contained some fractions of anhydrosugars and sugar polyols (Fig. 3h), as biomass burning can emit significant amounts of isoprene, α-pinene, and sugar polyols in winter (Akagi et al., 2011; Marynowski and Simoneit, 2022). An additional factor dominated by volatile n-alkanes and oxy-PAHs ($p_L^{0,*} > 10^{-8}$ atm) was resolved using the PMFw data (Fig. 3i). Given the presence of Ca^{2+} and SO_4^{2-}, this factor may indicate the partitioning of gaseous organics to PM and associated heterogeneous reactions. Unlike other factors associated with primary emissions (biomass burning, coal burning, dust, and lubricating oil combustion) or atmospheric processes (nitrate, sulfate, isoprene/α-pinene/biogenic SOA, and gas-surface interaction), the secondary NP production factor was not characterized by any OMM specifically related to sources. Due to the high loadings of 4NP, 3M4NP, and 2M4NP (Fig. 3f), the secondary NP production likely represents a combination of atmospheric processes, including emissions, formation and loss processes, and meteorology based on their diurnal variations. The contributions of each factor to individual NPs and $PM_{2.5}$ bulk components were illustrated using stack plots for the three sampling campaigns. As shown in Fig. 4 and S11–S13, the total contributions agreed with input measurements and reproduced the diurnal pattern for most species, supporting the robustness of the selected PMF solutions.

The distribution of factor contributions for NPs and $PM_{2.5}$ bulk components in winter was generally consistent across the three sampling campaigns. 4NP, 3M4NP, and 2M4NP in integrated and time-resolved $PM_{2.5}$ samples from northern Nanjing were mainly contributed by the secondary NP production factor (Fig. 4 and S11), whose diurnal pattern showed a slight increase at noon (12:00–14:00) due to photooxidation and a noticeable rise from 20:00 to 2:00 (next day) caused by nighttime NO_3· chemistry. The lubricating oil combustion factor contributed significantly to 4NP (14.4 %–25.7 %) only at urban sites in central YRD during winter (Fig. S12), as motor vehicle emissions are an important primary source of 4NP in urban areas (Yan et al., 2023a, b). With the inclusion of the day-night cycle, a significant fraction of 4NP (24.0 %–37.3 %) and 2M4NP (9.47 %–18.0 %) in time-resolved samples was apportioned to the gas-surface interaction factor (Fig. 4), which showed higher contributions during the daytime than at night. 4NC in all winter $PM_{2.5}$ samples was mainly (>80 %) attributed to the biomass burning factor, indicating the dominance of regional influence. Considering the high reactivity of NPs, the fractions assigned to biomass burning were likely immediate products from the atmospheric oxidation of biomass burning smoke.

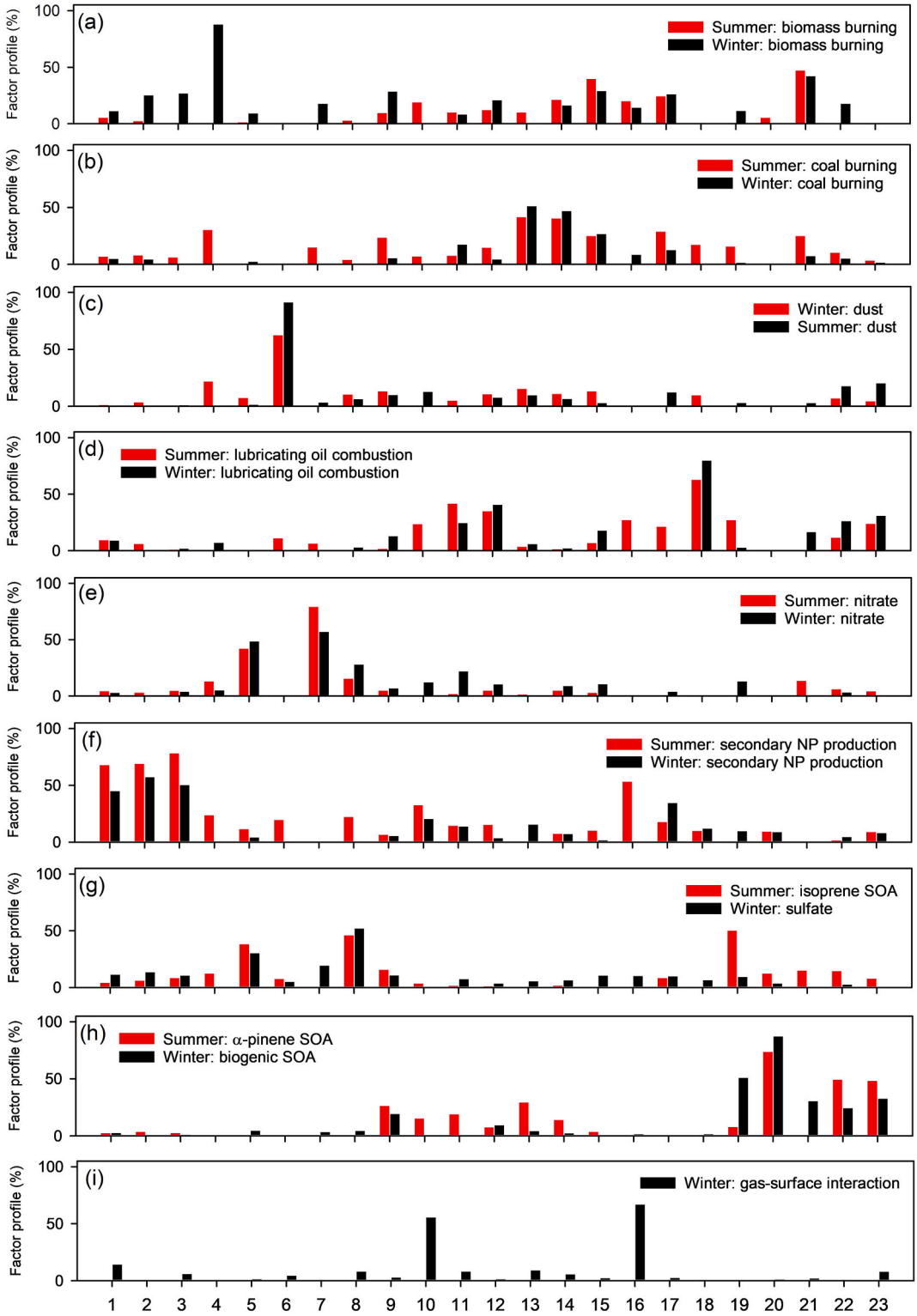

Fig. 3. Comparison of the normalized factor profiles between the 8-factor solution in summer and the 9-factor solution in winter
1. 4-Nitrophenol; 2. 3-Methyl-4-nitrophenol; 3. 2-Methyl-4-nitrophenol; 4. 4-Nitrocatechol; 5. NH_4^+; 6. Ca^{2+}; 7. NO_3^-; 8. SO_4^{2-}; 9. OC; 10. n-Alkanes lg $p_L^{o,*}$ (>−8); 11. n-Alkanes lg $p_L^{o,*}$ (−10 ~ −8); 12. n-Alkanes lg $p_L^{o,*}$ (<−10); 13. PAHs lg $p_L^{o,*}$ (>−8); 14. PAHs lg $p_L^{o,*}$ (−10 ~ −8); 15. PAHs lg $p_L^{o,*}$ (<−10); 16. oxy-PAHs lg $p_L^{o,*}$ (>−8); 17. oxy-PAHs lg $p_L^{o,*}$ (<−8); 18. Steranes and hopanes; 19. Isoprene SOA tracers; 20. α-Pinene SOA tracers; 21. Anhydrosugars; 22. Sugar alcohols; 23. Saccharides.

The summertime $PM_{2.5}$ bulk components were well explained and showed similar distributions of factor contributions for both integrated and time-resolved samples in northern Nanjing, but NPs were not consistently revealed between the two sampling campaigns. Due to the absence of the day-night cycle, NPs in integrated $PM_{2.5}$ samples were primarily apportioned to coal burning, sulfate, and nitrate factors (Fig. S11a). For time-resolved $PM_{2.5}$ samples, the total NPs were predominantly attributed to the secondary NP production factor (44.3 %–

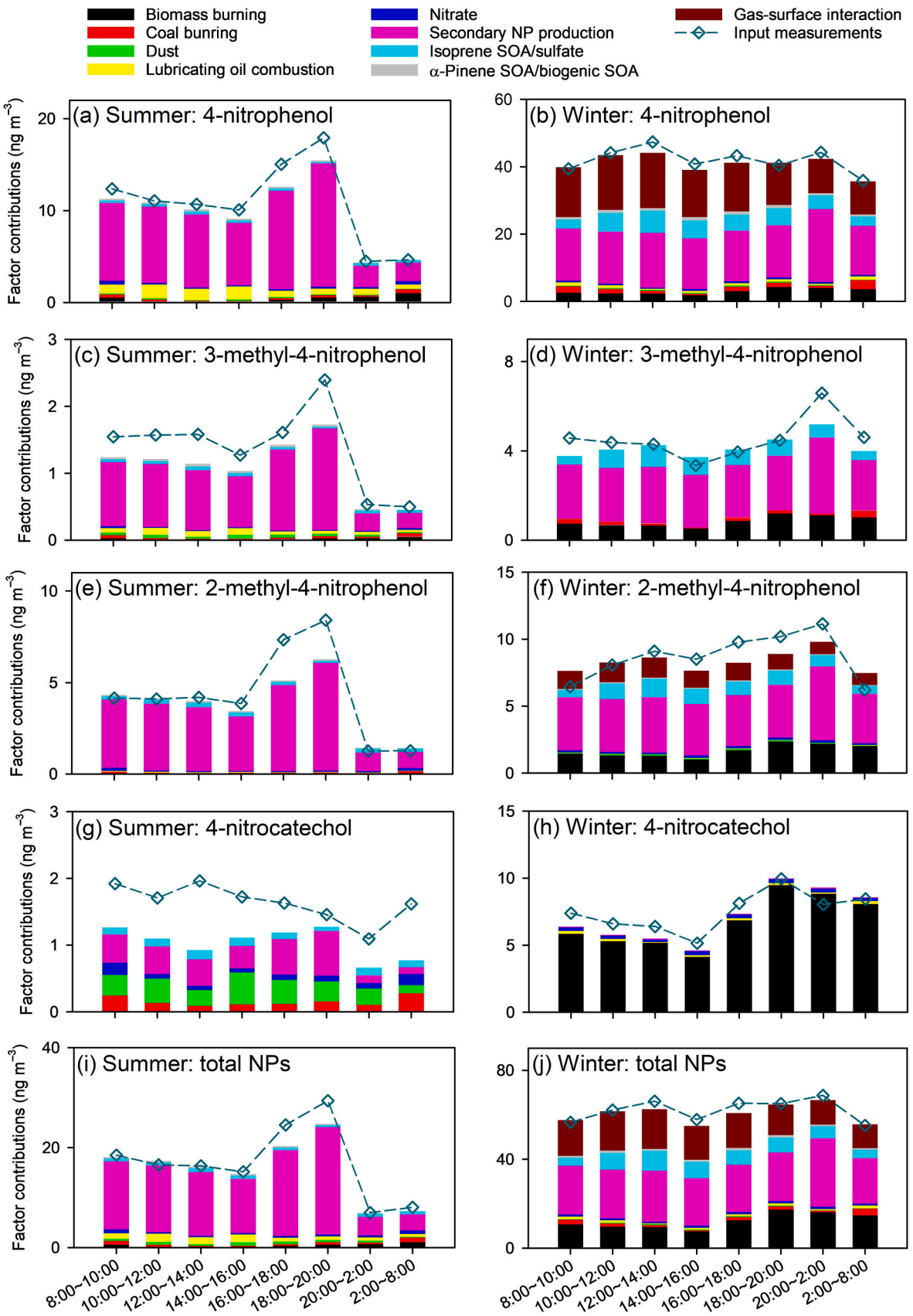

Fig. 4. Diurnal variations of stacked mean factor contributions to individual NPs in $PM_{2.5}$ from northern Nanjing in summer (July–August) and winter (January) 2019. The scatter data represent mean values of input measurements.

86.9 %, Fig. 4i). Except for 4NC, the diurnal profile of the secondary NP production factor almost reproduced those of NP concentrations. The discrepancy between the measured and simulated diurnal patterns for 4NC in summer (Fig. 4g) may be caused by the large fraction (55.4 %) of missed measurements for time-resolved samples. Because NP concentrations are controlled by their formation and degradation, none of the typical source markers used in this study can track their temporal variations in summer. Therefore, the identified secondary NP production factor is not a specific source for NPs but represents a combination of atmospheric processes.

4. Conclusions

In this work, PM samples from three sampling campaigns were analyzed to determine the size, spatial distribution, and diurnal variations of four NPs, including 4NP, 3M4NP, 2M4NP, and 4NC, in central YRD, China. Comparisons of NP concentrations between $PM_{2.5}$ and PM_{10} samples showed enrichment in fine particles during both summer and winter. Due to the evaporation of NPs at high temperatures, a greater fraction of NPs was observed in coarse PM in summer than in winter. In winter, individual NPs exhibited similar concentration time series across the five urban sites in central YRD, and 4NC had the lowest spatial variability, indicating significant regional influences. The diurnal variations of 4NP, 3M4NP, and 2M4NP in winter were driven by gas-phase photooxidation before noon, biomass burning for domestic heating in the late afternoon and early evening, and nighttime NO_3·-induced oxidation. Their summertime diurnal patterns reflected rapid formation during the evening rush hour and NO_3·-induced degradation. However, 4NC showed a different diurnal profile, resembling that of anhydrosugars in winter and secondary sulfate in summer. Combined with other speciation data of $PM_{2.5}$ samples, PMF analysis for both summer and winter identified a secondary NP production factor, which contributed most NPs in northern Nanjing. Since the diurnal pattern of the factor contribution was balanced by the formation and removal of NPs, the secondary NP production factor actually represented a combination of atmospheric processes. Considering the high reactivity of NPs in the atmosphere, the contribution of the biomass burning factor might indicate the immediate formation of NPs from the oxidation of biomass burning smoke.

CRediT authorship contribution statement

Chao Qin: Writing – original draft, Investigation, Data curation. **Jingyi Liu:** Investigation, Data curation. **Xinyu Ji:** Visualization, Investigation. **Wei Feng:** Validation, Investigation. **Zhijuan Shao:** Writing – review & editing. **Hong Liao:** Writing – review & editing, Resources. **Yuhang Wang:** Writing – review & editing, Resources. **Guofeng Shen:** Writing – review & editing. **Mingjie Xie:** Writing – review & editing, Supervision, Project administration, Methodology, Conceptualization.

Declaration of competing interest

The authors declare that they have no known competing financial interests or personal relationships that could have appeared to influence the work reported in this paper.

Acknowledgements

This work was supported by the National Natural Science Foundation of China (NSFC, 42577538, 42177211). We also thank the Nanjing Environmental Monitoring Center of Jiangsu Province for help with sampling.

Appendix A. Supplementary data

Supplementary data to this article can be found online at https://doi.org/10.1016/j.envpol.2025.127581.

Data availability

Data will be made available on request.

References

Abdelmoneim, M.S., Hafez, E.E., Dawood, M.F.A., Hammad, S.F., Ghazy, M.A., 2024. Toxicity of bisphenol A and p-nitrophenol on tomato plants: Morpho-physiological, ionomic profile, and antioxidants/defense-related gene expression studies. Biomol. Concepts 15. https://doi.org/10.1515/bmc-2022-0049.

Adamek, M., Kavčič, A., Debeljak, M., Šala, M., Grdadolnik, J., Vogel-Mikuš, K., Kroflič, A., 2024. Toxicity of nitrophenolic pollutant 4-nitroguaiacol to terrestrial plants and comparison with its non-nitro analogue guaiacol (2-methoxyphenol). Sci. Rep. 14, 2198. https://doi.org/10.1038/s41598-024-52610-6.

Akagi, S.K., Yokelson, R.J., Wiedinmyer, C., Alvarado, M.J., Reid, J.S., Karl, T., Crounse, J.D., Wennberg, P.O., 2011. Emission factors for open and domestic biomass burning for use in atmospheric models. Atmos. Chem. Phys. 11, 4039–4072. https://doi.org/10.5194/acp-11-4039-2011.

Barzaghi, P., Herrmann, H., 2004. Kinetics and mechanisms of reactions of the nitrate radical (NO3) with substituted phenols in aqueous solution. Phys. Chem. Chem. Phys. 6, 5379–5388. https://doi.org/10.1039/B412933D.

Chow, K.S., Huang, X.H.H., Yu, J.Z., 2015. Quantification of nitroaromatic compounds in atmospheric fine particulate matter in Hong Kong over 3 years: field measurement evidence for secondary formation derived from biomass burning emissions. Environ. Chem. 13, 665–673. https://doi.org/10.1071/EN15174.

Cui, T., Zeng, Z., Dos Santos, E.O., Zhang, Z., Chen, Y., Zhang, Y., Rose, C.A., Budisulistiorini, S.H., Collins, L.B., Bodnar, W.M., 2018. Development of a hydrophilic interaction liquid chromatography (HILIC) method for the chemical characterization of water-soluble isoprene epoxydiol (IEPOX)-derived secondary organic aerosol. Environ. Sci. Process. Impacts 20, 1524–1536. https://doi.org/10.1039/C8EM00308D.

Cui, W., Wang, Z., Feng, W., Qin, C., Liao, H., Wang, Y., Xie, M., 2025. Evaluating coarse PM composition and sources based on bulk and molecular speciation of PM2.5 and PM10 in Nanjing, East China. J. Environ. Sci. 152, 155–166. https://doi.org/10.1016/j.jes.2024.04.038.

Eichenbaum, G., Johnson, M., Kirkland, D., O'Neill, P., Stellar, S., Bielawne, J., DeWire, R., Areia, D., Bryant, S., Weiner, S., Desai-Krieger, D., Guzzie-Peck, P., Evans, D.C., Tonelli, A., 2009. Assessment of the genotoxic and carcinogenic risks of p-nitrophenol when it is present as an impurity in a drug product. Regul. Toxicol. Pharmacol. 55, 33–42. https://doi.org/10.1016/j.yrtph.2009.05.018.

Feng, W., Wang, X., Shao, Z., Liao, H., Wang, Y., Xie, M., 2023. Time-resolved measurements of $PM_{2.5}$ chemical composition and brown carbon absorption in Nanjing, East China: diurnal variations and organic tracer-based PMF analysis. J. Geophys. Res. Atmos. 128. https://doi.org/10.1029/2023JD039092 e2023JD039092.

Feng, W., Dong, G., Qi, W., Wang, Y., Zhang, X., Li, K., Liao, H., Wang, Y., Shao, Z., Xie, M., 2024. Spatiotemporal variations of PM2.5 organic molecular markers in five central cities of the Yangtze River Delta, East China in autumn and winter: implications for regional and local sources of organic aerosols. Environ. Pollut. 363, 125227. https://doi.org/10.1016/j.envpol.2024.125227.

Feng, W., Ding, F., Qi, W., Dong, G., Xie, M., 2025. Spatiotemporal distribution of light absorption of $PM_{2.5}$ organic carbon and its sources in urban areas in southern Jiangsu. Acta Sci. Circumstantiae 45, 331–340. https://doi.org/10.13671/j.hjkxxb.2024.0439.

Guo, Z., Hu, X., Sun, W., Peng, X., Fu, Y., Liu, K., Liu, F., Meng, H., Zhu, Y., Zhang, G., Wang, X., Xue, L., Wang, J., Wang, X., Peng, P.a., Bi, X., 2024. Mixing state and influence factors controlling diurnal variation of particulate nitrophenol compounds at a suburban area in northern China. Environ. Pollut. 344, 123368. https://doi.org/10.1016/j.envpol.2024.123368.

Inomata, S., Fushimi, A., Sato, K., Fujitani, Y., Yamada, H., 2015. 4-Nitrophenol, 1-nitropyrene, and 9-nitroanthracene emissions in exhaust particles from diesel vehicles with different exhaust gas treatments. Atmos. Environ. 110, 93–102. https://doi.org/10.1016/j.atmosenv.2015.03.043.

Kahnt, A., Behrouzi, S., Vermeylen, R., Safi Shalamzari, M., Vercauteren, J., Roekens, E., Claeys, M., Maenhaut, W., 2013. One-year study of nitro-organic compounds and their relation to wood burning in PM10 aerosol from a rural site in Belgium. Atmos. Environ. 81, 561–568. https://doi.org/10.1016/j.atmosenv.2013.09.041.

Khan, F., Jaoui, M., Rudziński, K., Kwapiszewska, K., Martinez-Romero, A., Gil-Casanova, D., Lewandowski, M., Kleindienst, T.E., Offenberg, J.H., Krug, J.D., Surratt, J.D., Szmigielski, R., 2022. Cytotoxicity and oxidative stress induced by atmospheric mono-nitrophenols in human lung cells. Environ. Pollut. 301, 119010. https://doi.org/10.1016/j.envpol.2022.119010.

Kim, E., Hopke, P.K., Pinto, J.P., Wilson, W.E., 2005. Spatial variability of fine particle mass, components, and source contributions during the regional air pollution study in St. Louis. Environ. Sci. Technol. 39, 4172–4179. https://doi.org/10.1021/es049824x.

Krudysz, M.A., Froines, J.R., Fine, P.M., Sioutas, C., 2008. Intra-community spatial variation of size-fractionated PM mass, OC, EC, and trace elements in the Long

Beach, CA area. Atmos. Environ. 42, 5374–5389. https://doi.org/10.1016/j.atmosenv.2008.02.060.
Laskin, A., Lin, P., Laskin, J., Fleming, L.T., Nizkorodov, S., 2018. Molecular characterization of atmospheric brown carbon, in: multiphase environmental chemistry in the atmosphere, ACS Symposium Series, 1299. Am. Chem. Soc. 261–274. https://doi.org/10.1021/bk-2018-1299.ch013.
Li, M., Wang, X., Lu, C., Li, R., Zhang, J., Dong, S., Yang, L., Xue, L., Chen, J., Wang, W., 2020a. Nitrated phenols and the phenolic precursors in the atmosphere in urban Jinan, China. Sci. Total Environ. 714, 136760. https://doi.org/10.1016/j.scitotenv.2020.136760.
Li, X., Wang, Y., Hu, M., Tan, T., Li, M., Wu, Z., Chen, S., Tang, X., 2020b. Characterizing chemical composition and light absorption of nitroaromatic compounds in the winter of Beijing. Atmos. Environ. 237, 117712. https://doi.org/10.1016/j.atmosenv.2020.117712.
Li, X., Jiang, L., Hoa, L.P., Lyu, Y., Xu, T., Yang, X., Iinuma, Y., Chen, J., Herrmann, H., 2016. Size distribution of particle-phase sugar and nitrophenol tracers during severe urban haze episodes in Shanghai. Atmos. Environ. 145, 115–127. https://doi.org/10.1016/j.atmosenv.2016.09.030.
Liang, Y., Wang, X., Dong, S., Liu, Z., Mu, J., Lu, C., Zhang, J., Li, M., Xue, L., Wang, W., 2020. Size distributions of nitrated phenols in winter at a coastal site in north China and the impacts from primary sources and secondary formation. Chemosphere 250, 126256. https://doi.org/10.1016/j.chemosphere.2020.126256.
Lin, P., Liu, J.M., Shilling, J.E., Kathmann, S.M., Laskin, J., Laskin, A., 2015. Molecular characterization of brown carbon (BrC) chromophores in secondary organic aerosol generated from photo-oxidation of toluene. Phys. Chem. Chem. Phys. 17, 23312–23325. https://doi.org/10.1039/c5cp02563j.
Lin, P., Aiona, P.K., Li, Y., Shiraiwa, M., Laskin, J., Nizkorodov, S.A., Laskin, A., 2016. Molecular characterization of brown carbon in biomass burning aerosol particles. Environ. Sci. Technol. 50, 11815–11824. https://doi.org/10.1021/acs.est.6b03024.
Liu, J., Lin, P., Laskin, A., Laskin, J., Kathmann, S.M., Wise, M., Caylor, R., Imholt, F., Selimovic, V., Shilling, J.E., 2016. Optical properties and aging of light-absorbing secondary organic aerosol. Atmos. Chem. Phys. 16, 12815–12827. https://doi.org/10.5194/acp-16-12815-2016.
Lu, C., Wang, X., Li, R., Gu, R., Zhang, Y., Li, W., Gao, R., Chen, B., Xue, L., Wang, W., 2019a. Emissions of fine particulate nitrated phenols from residential coal combustion in China. Atmos. Environ. 203, 10–17. https://doi.org/10.1016/j.atmosenv.2019.01.047.
Lu, C., Wang, X., Dong, S., Zhang, J., Li, J., Zhao, Y., Liang, Y., Xue, L., Xie, H., Zhang, Q., Wang, W., 2019b. Emissions of fine particulate nitrated phenols from various on-road vehicles in China. Environ. Res. 179, 108709. https://doi.org/10.1016/j.envres.2019.108709.
Marynowski, L., Simoneit, B.R.T., 2022. Saccharides in atmospheric particulate and sedimentary organic matter: status overview and future perspectives. Chemosphere 288, 132376. https://doi.org/10.1016/j.chemosphere.2021.132376.
Mo, L., Wang, X., Liao, Y., Liu, Y., Tang, A., Li, J., Yang, P., 2024. Environmental pollutant 3-methyl-4-nitrophenol promotes the expression of oncostatin M to exacerbate airway allergic inflammation. Clin. Exp. Immunol. 218, 111–119. https://doi.org/10.1093/cei/uxae078.
Mohr, C., Lopez-Hilfiker, F.D., Zotter, P., Prévôt, A.S.H., Xu, L., Ng, N.L., Herndon, S.C., Williams, L.R., Franklin, J.P., Zahniser, M.S., Worsnop, D.R., Knighton, W.B., Aiken, A.C., Gorkowski, K.J., Dubey, M.K., Allan, J.D., Thornton, J.A., 2013. Contribution of nitrated phenols to wood burning brown carbon light absorption in Detling, United Kingdom during winter time. Environ. Sci. Technol. 47, 6316–6324. https://doi.org/10.1021/es400683v.
Nakayama, T., Matsumi, Y., Sato, K., Imamura, T., Yamazaki, A., Uchiyama, A., 2010. Laboratory studies on optical properties of secondary organic aerosols generated during the photooxidation of toluene and the ozonolysis of α-pinene. J. Geophys. Res. Atmos. 115. https://doi.org/10.1029/2010jd014387.
Offenberg, J.H., Baker, J.E., 1999. Aerosol size distributions of polycyclic aromatic hydrocarbons in urban and over-water atmospheres. Environ. Sci. Technol. 33, 3324–3331. https://doi.org/10.1021/es990089c.
Pang, H., Zhang, Q., Lu, X., Li, K., Chen, H., Chen, J., Yang, X., Ma, Y., Ma, J., Huang, C., 2019. Nitrite-mediated photooxidation of vanillin in the atmospheric aqueous phase. Environ. Sci. Technol. 53, 14253–14263. https://doi.org/10.1021/acs.est.9b03649.
Qi, L., Wang, S., 2019. Fossil fuel combustion and biomass burning sources of global black carbon from GEOS-Chem simulation and carbon isotope measurements. Atmos. Chem. Phys. 19, 11545–11557. https://doi.org/10.5194/acp-19-11545-2019.
Sakakibara, K., Taira, M., Nagatomi, K., Kuriyama, G., Ohira, S.-I., Toda, K., 2022. Diurnal variations of gaseous and particulate nitrophenol isomers in the atmosphere monitored by using wet scrubbing online preconcentration. Environ. sci. Atmos. 2, 1108–1119. https://doi.org/10.1039/D2EA00021K.
Simoneit, B.R.T., Elias, V.O., Kobayashi, M., Kawamura, K., Rushdi, A.I., Medeiros, P.M., Rogge, W.F., Didyk, B.M., 2004. Sugars–Dominant water-soluble organic compounds in soils and characterization as tracers in atmospheric particulate matter. Environ. Sci. Technol. 38, 5939–5949. https://doi.org/10.1021/es0403099.
Surratt, J.D., Chan, A.W.H., Eddingsaas, N.C., Chan, M., Loza, C.L., Kwan, A.J., Hersey, S.P., Flagan, R.C., Wennberg, P.O., Seinfeld, J.H., 2010. Reactive intermediates revealed in secondary organic aerosol formation from isoprene. Proc. Natl. Acad. Sci. USA 107, 6640–6645. https://doi.org/10.1073/pnas.0911114107.
Teich, M., van Pinxteren, D., Wang, M., Kecorius, S., Wang, Z., Müller, T., Močnik, G., Herrmann, H., 2017. Contributions of nitrated aromatic compounds to the light absorption of water-soluble and particulate brown carbon in different atmospheric environments in Germany and China. Atmos. Chem. Phys. 17, 1653–1672. https://doi.org/10.5194/acp-17-1653-2017.
Verma, S.K., Kawamura, K., Chen, J., Fu, P., 2018. Thirteen years of observations on primary sugars and sugar alcohols over remote Chichijima Island in the Western North Pacific. Atmos. Chem. Phys. 18, 81–101. https://doi.org/10.5194/acp-18-81-2018.
Vidović, K., Lašič Jurković, D., Šala, M., Kroflič, A., Grgić, I., 2018. Nighttime aqueous-phase formation of nitrocatechols in the atmospheric condensed phase. Environ. Sci. Technol. 52, 9722–9730. https://doi.org/10.1021/acs.est.8b01161.
Wang, G., Kawamura, K., Xie, M., Hu, S., Gao, S., Cao, J., An, Z., Wang, Z., 2009. Size-distributions of n-alkanes, PAHs and hopanes and their sources in the urban, mountain and marine atmospheres over East Asia. Atmos. Chem. Phys. 9, 8869–8882. https://doi.org/10.5194/acp-9-8869-2009.
Wang, H., Gao, Y., Wang, S., Wu, X., Liu, Y., Li, X., Huang, D., Lou, S., Wu, Z., Guo, S., Jing, S., Li, Y., Huang, C., Tyndall, G.S., Orlando, J.J., Zhang, X., 2020. Atmospheric processing of nitrophenols and nitrocresols from biomass burning emissions. J. Geophys. Res. Atmos. 125. https://doi.org/10.1029/2020JD033401 e2020JD033401.
Wang, J., 2013. China air quality online monitoring and analysis platform. http://www.aqistudy.cn. (Accessed 27 November 2025).
Wang, L., Wang, X., Gu, R., Wang, H., Yao, L., Wen, L., Zhu, F., Wang, W., Xue, L., Yang, L., Lu, K., Chen, J., Wang, T., Zhang, Y., Wang, W., 2018. Observations of fine particulate nitrated phenols in four sites in northern China: concentrations, source apportionment, and secondary formation. Atmos. Chem. Phys. 18, 4349–4359. https://doi.org/10.5194/acp-18-4349-2018.
Wang, S., Li, H., 2021. NO3·-initiated gas-phase formation of nitrated phenolic compounds in polluted atmosphere. Environ. Sci. Technol. 55, 2899–2907. https://doi.org/10.1021/acs.est.0c08041.
Wang, X., Gu, R., Wang, L., Xu, W., Zhang, Y., Chen, B., Li, W., Xue, L., Chen, J., Wang, W., 2017. Emissions of fine particulate nitrated phenols from the burning of five common types of biomass. Environ. Pollut. 230, 405–412. https://doi.org/10.1016/j.envpol.2017.06.072.
Wilson, J.G., Kingham, S., Pearce, J., Sturman, A.P., 2005. A review of intraurban variations in particulate air pollution: implications for epidemiological research. Atmos. Environ. 39, 6444–6462. https://doi.org/10.1016/j.atmosenv.2005.07.030.
Wongphatarakul, V., Friedlander, S.K., Pinto, J.P., 1998. A comparative study of PM2.5 ambient aerosol chemical databases. Environ. Sci. Technol. 32, 3926–3934. https://doi.org/10.1021/es9800582.
Xie, M., Chen, X., Hays, M.D., Holder, A.L., 2019a. Composition and light absorption of N-containing aromatic compounds in organic aerosols from laboratory biomass burning. Atmos. Chem. Phys. 19, 2899–2915. https://doi.org/10.5194/acp-19-2899-2019.
Xie, M., Chen, X., Hays, M.D., Lewandowski, M., Offenberg, J., Kleindienst, T.E., Holder, A.L., 2017. Light absorption of secondary organic aerosol: composition and contribution of nitroaromatic compounds. Environ. Sci. Technol. 51, 11607–11616. https://doi.org/10.1021/acs.est.7b03263.
Xie, M., Peng, X., Shang, Y., Yang, L., Zhang, Y., Wang, Y., Liao, H., 2022. Collocated measurements of light-absorbing organic carbon in $PM_{2.5}$: observation uncertainty and organic tracer-based source apportionment. J. Geophys. Res. Atmos. 127. https://doi.org/10.1029/2021JD035874 e2021JD035874.
Xie, M., Chen, X., Holder, A.L., Hays, M.D., Lewandowski, M., Offenberg, J.H., Kleindienst, T.E., Jaoui, M., Hannigan, M.P., 2019b. Light absorption of organic carbon and its sources at a southeastern U.S. location in summer. Environ. Pollut. 244, 38–46. https://doi.org/10.1016/j.envpol.2018.09.125.
Xie, M., Zhao, Z., Holder, A.L., Hays, M.D., Chen, X., Shen, G., Jetter, J.J., Champion, W. M., Wang, Q., 2020. Chemical composition, structures, and light absorption of N-containing aromatic compounds emitted from burning wood and charcoal in household cookstoves. Atmos. Chem. Phys. 20, 14077–14090. https://doi.org/10.5194/acp-20-14077-2020.
Yan, J., Wang, X., Gao, S., Gong, P., Dotel, J., Pokhrel, B., 2023a. Diagnostic ratio of nitrated phenols as a new method for the identification of pollution emission sources. Environ. Pollut. 316, 120509. https://doi.org/10.1016/j.envpol.2022.120509.
Yan, J., Wang, X., Gao, S., Gong, P., Liu, X., Xu, T., Dotel, J., Pokhrel, B., 2023b. Light absorption of brown carbon and nitrated phenols in aerosols in a city of South Asia: from sources to atmosphere. Appl. Geochem. 152, 105666. https://doi.org/10.1016/j.apgeochem.2023.105666.
Yu, Y., He, S., Wu, X., Zhang, C., Yao, Y., Liao, H., Wang, Q.g., Xie, M., 2019. $PM_{2.5}$ elements at an urban site in Yangtze River Delta, China: high time-resolved measurement and the application in source apportionment. Environ. Pollut. 253, 1089–1099. https://doi.org/10.1016/j.envpol.2019.07.096.
Yuan, W., Huang, R.J., Yang, L., Wang, T., Duan, J., Guo, J., Ni, H., Chen, Y., Chen, Q., Li, Y., Dusek, U., O'Dowd, C., Hoffmann, T., 2021. Measurement report: $PM_{2.5}$-bound nitrated aromatic compounds in Xi'an, Northwest China – seasonal variations and contributions to optical properties of brown carbon. Atmos. Chem. Phys. 21, 3685–3697. https://doi.org/10.5194/acp-21-3685-2021.
Zhang, X., Lin, Y.-H., Surratt, J.D., Weber, R.J., 2013. Sources, composition and absorption Ångström exponent of light-absorbing organic components in aerosol extracts from the Los Angeles Basin. Environ. Sci. Technol. 47, 3685–3693. https://doi.org/10.1021/es305047b.

Zhang, X., Liu, H., Cheng, J., Song, W., Wang, H., Zhang, Y., Wang, X., 2025. Gas-phase oxidation of guaiacol by NO_3 radicals: kinetic measurements and implications. ACS ES&T Air 2, 903–910. https://doi.org/10.1021/acsestair.4c00353.
Zhang, Y.Y., Müller, L., Winterhalter, R., Moortgat, G.K., Hoffmann, T., Pöschl, U., 2010. Seasonal cycle and temperature dependence of pinene oxidation products, dicarboxylic acids and nitrophenols in fine and coarse air particulate matter. Atmos. Chem. Phys. 10, 7859–7873. https://doi.org/10.5194/acp-10-7859-2010.
Zhao, R., Lee, A.K.Y., Huang, L., Li, X., Yang, F., Abbatt, J.P.D., 2015. Photochemical processing of aqueous atmospheric brown carbon. Atmos. Chem. Phys. 15, 6087–6100. https://doi.org/10.5194/acp-15-6087-2015.